

Tuning infrared absorption in hyperbolic polaritons coated silk fibril composite

Lihong Shi(史丽弘), and Jiebin Peng(彭洁彬)

Citation: Chin. Phys. B, 2022, 31 (**11**): 114401. DOI: 10.1088/1674-1056/ac8cdc

What follows is a list of articles you may be interested in

Uniformity principle of temperature difference field in heat transfer optimization

Xue-Tao Cheng(程雪涛), Xin-Gang Liang(梁新刚)

Chin. Phys. B, 2019, 28 (**6**): 064402. DOI: 10.1088/1674-1056/28/6/064402

Spectral enhancement of thermal radiation by laser fabricating grating structure on nickel surface

Liu Song (刘嵩), Liu Shi-Bing (刘世炳)

Chin. Phys. B, 2015, 24 (**5**): 054401. DOI: 10.1088/1674-1056/24/5/054401

Near-field radiative heat transfer in mesoporous alumina

Li Jing (李静), Feng Yan-Hui (冯妍卉), Zhang Xin-Xin (张欣欣), Huang Cong-Liang (黄丛亮), Wang Ge (王戈)

Chin. Phys. B, 2015, 24 (**1**): 014401. DOI: 10.1088/1674-1056/24/1/014401

A comparison of different entransy flow definitions and entropy generation in thermal radiation optimization

Zhou Bing (周兵), Cheng Xue-Tao (程雪涛), Liang Xin-Gang (梁新刚)

Chin. Phys. B, 2013, 22 (**8**): 084401. DOI: 10.1088/1674-1056/22/8/084401

Thermal conductivity of a kind of mesoporous silica SBA-15

Huang Cong-Liang (黄丛亮), Feng Yan-Hui (冯妍卉), Zhang Xin-Xin (张欣欣), Li Jing (李静), Wang Ge (王戈)

Chin. Phys. B, 2013, 22 (**6**): 064401. DOI: 10.1088/1674-1056/22/6/064401

Tuning infrared absorption in hyperbolic polaritons coated silk fibril composite

Lihong Shi(史丽弘)[1,†] and Jiebin Peng(彭洁彬)[2,‡]

[1] *School of Science, JiangNan University, Wuxi* 214122, *China*

[2] *School of Physics and Optoelectronic Engineering, Guangdong University of Technology, Guangzhou* 510006, *China*

(Received 14 May 2022; revised manuscript received 21 July 2022; accepted manuscript online 26 August 2022)

Advanced textiles for thermal management give rise to many functional applications and unveil a new frontier for the study of human thermal comfort. Manipulating the coated quasi-particles between the composite components offers a platform to study the advanced thermoregulatory textiles. Here, we propose that coating the hyperbolic polariton can be an effective tool to tune infrared absorption in hexagonal boron nitride-coated silk composite. Remarkably, we achieve significant tuning of the infrared absorption efficiency of silk fibrils through the designed hexagonal boron nitride film. The underlying mechanism is related to resonance coupling between hyperbolic phonon polaritons. We find a notably high infrared absorption efficiency, nearly 3 orders larger than that without hBN coating, which can be achieved in our composite system. Our results indicate the promising future of advanced polariton-coated textiles and open a pathway to guide the artificial-intelligence design of advanced functional textiles.

Keywords: thermal radiation, thermal management, infrared absorption, hyperbolic polaritons

PACS: 44.40.+a, 65.90.+i, 33.20.Ea, 71.36.+c **DOI:** 10.1088/1674-1056/ac8cdc

Human thermal comfort can be regarded as the state in which the surface temperature of the skin is converging on the normal body temperature as much as possible. Thermal comfort is associated with multiple heat transfer pathways among skin, textile, sun and the external environment.[1–4] We can achieve thermal comfort by external active equipment, such as air-conditioning, fans and heaters. Except for those active strategies, it is found that improving the personal microclimate is an effective way to enhance human thermal comfort and reduce unnecessary energy consumption. We can consider the mechanism of heat transfer and manage the heat transfer rate between the clothed skin and environment to regulate the personal microclimate effectively. However, the heat transfer rates in human thermal comfort mainly depend on the design of textiles, and traditional textiles cannot flexibly regulate human heat dissipation in cold and hot conditions.[5–7] Consequently, researchers have explored advanced thermoregulatory textiles to achieve thermal comfort for the human body, such as warming textiles using metals with high reflectance in the field of textiles. Due to the lack of breathability, these warming textiles are not comfortable to wear. Hsu *et al.* developed a high-cost warming textile using cotton with embedded metallic silver nanowires to overcome the shortcut of breathability.[8] In addition, Hazarika *et al.* designed a Woven Kevlar fiber by developing copper–nickel (Cu–Ni) nanowires on the WKF surface in a complicated preparative process to reduce the cost.[9] However, these approaches for warming textiles have the disadvantage of mass production. Except for the above methods with reflectivity regulation, some researchers have proposed utilizing solar energy to enhance the warming effect of textiles. Luo *et al.* made a colored warming textile using a lossy dielectric layer and a metal layer to coat with nanoporous textile.[10] In this design, the metal layer can largely reduce the emittance of the outer surface in the visible band, and the lossy dielectric layer can absorb a large amount of solar energy in the near infrared band. Zhu *et al.* presented that by coating the exterior and interior of the enclosure roof with two visible-transparent films with distinctive wavelength selectivity, they can implement simultaneous control over the energy exchange among the enclosure with the hot sun, the cold outer space, the atmosphere and the active cooler.[11] Luo *et al.* reported that an eco-friendly passive nanostructured textile can harvest energy from the sun and the outer space for tunable control of heating and cooling. Under sunlight exposure, its heating and cooling mode is able to make a skin simulator temperature increase/decrease of 8.1 °C/6 °C, respectively.[12] It is a promising way for advanced thermoregulatory textiles to use solar energy in the development of warming textiles. Nevertheless, there are few studies based on the concept of improving the infrared absorption of textiles.

In thermal regulation applications, boron nitride (BN) has been considered as an effective two-dimensional (2D) material because of its high thermal conductance and electrical insulation. For instance, a composite fiber with BN nanosheets can provide external radiative heat transfer channels for body heat

†Corresponding author. E-mail: lihong@jiangnan.edu.cn

‡Corresponding author. E-mail: pengjiebin@hotmail.com

© 2022 Chinese Physical Society and IOP Publishing Ltd

dissipation due to its highly confined phonon polaritons.[13–17] Several experimental results show that a composite fiber with a-BN/PVA has excellent thermal conductance.[18] Moreover, silk, as one of the most natural materials, has attracted much attention due to its excellent biological properties, such as degradability, good biocompatibility, water vapor permeability, and excellent oxygen.[19–21] Composites consisting of silk and carbon-based materials have shown promising applications in food processing and engineering,[22] tissue engineering and wearable devices.[23,24] In our previous work, we have found that the infrared absorption efficiency of silk fibrils with a graphene coating can be five orders of magnitude larger than that without a graphene coating due to the help of plasmon polaritons.[25] Analogous concepts can be explored in silk/hBN composite for advanced thermoregulatory textiles.

In this paper, we propose to design a silk/hBN composite to manipulate infrared radiation for tunable thermal absorption. We analyze the infrared radiation in hBN-coated silk composites in detail based on Mie scattering theory. We also study the impact of the thickness of the hexagonal boron nitride (hBN) film and radius of the silk nanofibrils on the absorption efficiency. We also provided an optimal thickness of hBN film for the best optical performance of nanocomposites.

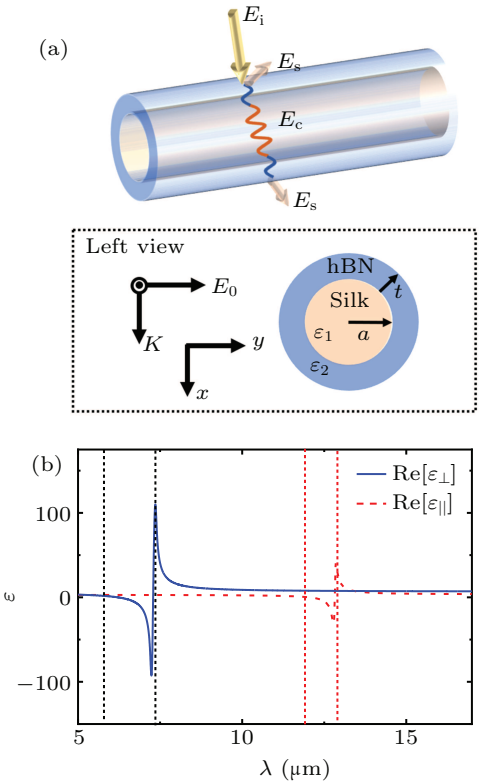


Fig. 1. (a) Schematic figure of our simulation model. A transverse electric field normally incident onto a long hBN-coated silk nanofibril, the radius of silk nanofibril is a. (b) Real part of the out-of-plane and in-plane dielectric functions of hBN *versus* light wavelength. The dashed lines show the hyperbolic regions of hBN.

As shown in Fig. 1(a), we consider a long hBn-coated silk nanofibril composite with radius of a. The BN/silk textile can be fabricated by a fast and scalable three-dimensional (3D) printing method, by which the BN/poly (vinyl alcohol) fiber has been realized in Ref. [18]. The 3D printing fabrication process of the BN/silk composite fibers can be illustrated as follows: first, liquid-phase exfoliated BN nanosheets can be prepared by sonicating raw hBN powders in isopropyl alcohol solution. Then, the raw hBN bulk powders can be exfoliated to BN flakes. After exfoliation, the (100), (101), and (102) peaks of the hBN bulk disappear, and the hBN micropowders can be successfully exfoliated to thin BN nanosheets. Uniform BN/silk suspensions can be obtained by dispersing liquid-phase exfoliated BN nanosheets into a silk dimethyl sulfoxide solution using sonication. Finally, the homogeneous BN/silk dispersion solution can be injected into a coagulation bath from a needle by the 3D printer to fabricate the continuous as-printed fibers.

A transverse electric field normally incident onto the silk nanofibril composite and the relative permittivity of silk and the host medium (air) are set to be $\varepsilon = 4.2$ and $\varepsilon_h = 1$, respectively.[26] The incident electric field is given as, $\boldsymbol{E} = E_0 \mathrm{e}^{\mathrm{i}k_0 x} \times \mathrm{e}^{-\mathrm{i}\omega t}\boldsymbol{y}$, where $k_0 = \omega\sqrt{\varepsilon_0\mu_0}$ is the wavenumber in free space.

The hBN film is a uniaxial dielectric material (bandgap ~ 5.9 eV) in the infrared region. When the optical axis is located in the z direction, the hBN film has two mid-infrared Reststrahlen bands. When the electric field is perpendicular to the optical axis, the in-plane dielectric function includes the contribution from in-plane phonon vibrations ($\omega_{\mathrm{TO},\perp} = 1370\ \mathrm{cm}^{-1}$, and $\omega_{\mathrm{LO},\perp} = 1610\ \mathrm{cm}^{-1}$). When the electric field is parallel to the optical axis, the out-plane dielectric function includes the contribution from out-plane phonon vibrations ($\omega_{\mathrm{TO},\parallel} = 780\ \mathrm{cm}^{-1}$ and $\omega_{\mathrm{LO},\parallel} = 830\ \mathrm{cm}^{-1}$). The dielectric function can be expressed as follows:[27–30]

$$\varepsilon_m = \varepsilon_{\infty,m}\left(1 + \frac{\omega_{\mathrm{LO},m}^2 - \omega_{\mathrm{TO},m}^2}{\omega_{\mathrm{TO},m}^2 - \mathrm{i}\gamma_m\omega - \omega^2}\right), \tag{1}$$

where $m = \parallel, \perp$ are the out-plane and the in-plane directions, respectively. The other parameters used here are $\varepsilon_{\infty,\parallel} = 2.95$ and $\gamma_\parallel = 4\ \mathrm{cm}^{-1}$, $\varepsilon_{\infty,\perp} = 4.87$ and $\gamma_\perp = 5\ \mathrm{cm}^{-1}$. Figure 1(b) shows the real part of the in-plane and out-plane dielectric functions of hBN in frequency space. The dashed lines show that the dielectric function can become negative in the Reststrahlen band between the TO and LO phonon modes. Thus, the in-plane and out-plane dielectric functions of hBN have opposite signs in each Restrahlen band and form a hyperbolic band.

For 2D materials, when the layer thickness is much smaller than the polariton wavelength, we can model the layer as a 2D isotropic conductivity layer with zero thickness. The effective conductivity of 2D materials is written as $\sigma_{\mathrm{eff}} = (ct/2\mathrm{i}\lambda_0)\varepsilon$, where c is the light velocity, λ_0 is the incident light wavelength, ε is the dielectric permittivity of the layer, and t is the thickness of the 2D layer.[31] The thickness of the hBN

film t considered here is approximately 5 nm–100 nm, which is much smaller than its polariton wavelength. Therefore, it is reasonable to model the hBN film by an isotropic in-plane conducting layer. The effective two-dimensional conductivity of the hBN film can be written as $\sigma_{\rm eff} = (ct/2{\rm i}\lambda_0)\varepsilon_\perp$, where $\varepsilon_\perp$ is the in-plane dielectric permittivity without considering the contribution of the out-of-plane part of the dielectric permittivity.

We apply Mie scattering theory to investigate light scattering in cylinders, which has been widely used in coated core-shell particles[32–34] and graphene/silk composite.[25] According to Mie scattering theory,[35–37] the electric field and magnetic field can be given by

$$\begin{aligned}
\boldsymbol{E}_{\rm i} &= -\frac{\rm i}{k_h}\sum_{n=-\infty}^{\infty} E_n \boldsymbol{M}_n^{(1)},\\
\boldsymbol{H}_{\rm i} &= \frac{-1}{\omega\mu_0}\sum_{n=-\infty}^{\infty} E_n \boldsymbol{N}_n^{(1)};\\
\boldsymbol{E}_{\rm s} &= -\frac{\rm i}{k_0}\sum_{n=-\infty}^{\infty} a_n E_n \boldsymbol{M}_n^{(3)},\\
\boldsymbol{H}_{\rm s} &= \frac{\rm i}{\omega\mu_0}\sum_{n=-\infty}^{\infty} a_n E_n \boldsymbol{N}_n^{(3)};
\end{aligned}$$

$$\begin{aligned}
\boldsymbol{E}_{\rm c} &= -\frac{\rm i}{k}\sum_{n=-\infty}^{\infty} b_n E_n \boldsymbol{M}_n^{(1)},\\
\boldsymbol{H}_{\rm c} &= \frac{\rm i}{\omega\mu}\sum_{n=-\infty}^{\infty} b_n E_n \boldsymbol{N}_n^{(1)},
\end{aligned} \tag{2}$$

where $E_n = E_0(-{\rm i})^n$ and $k = k_0\sqrt{\varepsilon}$, $\boldsymbol{M}_n$ and $\boldsymbol{N}_n$ are vector cylindrical harmonics. $\boldsymbol{E}_{\rm i}$, $\boldsymbol{E}_{\rm c}$, $\boldsymbol{E}_{\rm s}$ and $\boldsymbol{H}_{\rm i}$, $\boldsymbol{H}_{\rm c}$, $\boldsymbol{H}_{\rm s}$ are the incident, core, and scattering electric fields and magnetic fields, respectively. a_n and b_n are the scattering coefficient and the coefficient of the core field, respectively. The upper indices (1) and (3) are the Bessel function ${\rm J}_n$ and the first kind of Hankel function ${\rm H}_n$, respectively. The permeability of all the mediums is 1 ($\mu = \mu_0 = 1$).

For such a cylinder with the effective surface conductivity $\sigma_{\rm eff}$, the boundary condition can be given as follows:

$$\hat{\boldsymbol{n}}\cdot(\boldsymbol{E}_{\rm i}+\boldsymbol{E}_{\rm s}-\boldsymbol{E}_{\rm c}) = 0, \quad \hat{\boldsymbol{n}}\times(\boldsymbol{H}_{\rm c}-\boldsymbol{H}_{\rm i}-\boldsymbol{H}_{\rm s}) = \sigma_{\rm eff}\boldsymbol{E}_t. \tag{3}$$

By applying the boundary conditions at $r = a$, we can obtain the scattering coefficient as follows:

$$a_n = \frac{-{\rm J}_n'(k_0a)t_n + {\rm J}_n(k_0a){\rm J}_n'(ka)}{{\rm H}_n'(k_0a)t_n - {\rm H}_n(k_0a){\rm J}_n'(ka)}, \qquad F_n = \frac{{\rm H}_n(k_0a){\rm J}_n'(k_0a) - {\rm H}_n'(k_0a){\rm J}_n(k_0a)}{{\rm H}_n'(k_0a){\rm J}_n'(ka) - \sqrt{\varepsilon}{\rm H}_n'(k_0a){\rm J}_n(ka) - {\rm i}\sigma_{\rm eff}\eta_0{\rm H}_n'(k_0a){\rm J}_n'(ka)}, \tag{4}$$

where $\eta_0 = \sqrt{\mu_0/\varepsilon_0}$ is the impedance of free space. $t_n = \sqrt{\varepsilon}{\rm J}_n(k_0a) + {\rm i}\sigma_{\rm eff}\eta_0{\rm J}_n'(k_0a)$. The local electric fields within the dielectric cylinder can be obtained by substituting Eq. (4) into Eq. (2). At $r = a$, we can obtain the local fields near the silk–hBN interface,

$$E_{\rm c,local} = -E_0\sum_{n=-\infty}^{\infty}{\rm i}^{n+1}F_n\left({\rm i}n\frac{{\rm J}_n(ka)}{ka}e_r - {\rm J}_n'(ka)e_\varphi\right){\rm e}^{{\rm i}n\varphi}.$$

The square of the modulus of the local fields is expressed as follows:

$$\begin{aligned}
&\left|E_{\rm c,local}\right|^2\\
&= -|E_0|^2\left|\sum_{n=-\infty}^{\infty}{\rm i}^{n+1}F_n\left({\rm i}n\frac{{\rm J}_n(ka)}{ka}e_r - {\rm J}_n'(ka)e_\varphi\right){\rm e}^{{\rm i}n\varphi}\right|^2.
\end{aligned} \tag{5}$$

Then, the square of the modulus of the tangential local field within the hBN film

$$\left|E_{\rm lin,hBN}\right|^2 = -|E_0|^2\left|\sum_{n=-\infty}^{\infty}{\rm i}^{n+1}F_n{\rm J}_n'(ka)e_\varphi{\rm e}^{{\rm i}n\varphi}\right|^2. \tag{6}$$

Finally, we can obtain the scattering efficiency and extinction efficiency as follows:

$$\begin{aligned}
Q_{\rm sca} &= \frac{2}{k_0a}(|a_0|^2 + 2\sum_{n=1}^{\infty}|a_n|^2),\\
Q_{\rm ext} &= \frac{2}{k_0a}{\rm Re}(a_0 + 2\sum_{n=1}^{\infty}a_n).
\end{aligned} \tag{7}$$

We consider the incident light wavelength in the infrared region ($\sim$ μm), and the diameter of the silk nanofibrils observed in the experiment is in the range of several to tens of nanometers.[37] Because the incident light wavelength is much larger than the radius of silk ($\lambda \gg a$), we can obtain the electric potential both inside ($\phi_{\rm c}$) and outside ($\phi_{\rm h}$) the cylinders, which satisfy the Laplace equation: $\nabla^2\phi_{\rm c,h} = 0$.

Then, we can achieve the general solutions:

$$\begin{aligned}
\phi_{\rm c} &= -BE_0r\cos\varphi,\\
\phi_{\rm h} &= \left(-E_0r + \frac{CE_0}{r}\right)\cos\varphi.
\end{aligned} \tag{8}$$

To solve the coefficients B and C, we can apply the boundary conditions:

$$\begin{aligned}
\boldsymbol{n}\times[\boldsymbol{E}_{\rm h} - \boldsymbol{E}_{\rm c}]|_{r=a} &= 0,\\
\boldsymbol{n}\cdot[\boldsymbol{D}_{\rm h} - \boldsymbol{D}_{\rm c}]|_{r=a} &= \rho,
\end{aligned} \tag{9}$$

where $\boldsymbol{E}_{\rm c,h} = -\nabla\phi_{\rm c,h}$ and $\boldsymbol{D}_{\rm c,h} = \varepsilon_{\rm c,h}\boldsymbol{E}_{\rm c,h}$ are the electric field and electric displacement vector inside and outside the cylinder, respectively. ρ represents the surface charges and has ${\rm i}\omega\rho = \nabla\cdot\boldsymbol{J}$ the relation with the surface $\boldsymbol{J}$ current density.

Combining Eqs. (8) and (9), we can obtain

$$B = \frac{2\varepsilon_{\rm h}}{\varepsilon+\varepsilon_{\rm h}+\gamma}, \quad C = \frac{a^2(\varepsilon-\varepsilon_{\rm h}+\gamma)}{\varepsilon+\varepsilon_{\rm h}+\gamma}, \tag{10}$$

where

$$\gamma = \frac{\mathrm{i}\sigma_{\mathrm{eff}}}{\omega a \varepsilon_0}.$$

In the connection with $E_{\mathrm{c}} = -\nabla\phi_{\mathrm{c}} = BE_0(\cos\varphi \boldsymbol{e}_r - \sin\varphi \boldsymbol{e}_\varphi)$.

We can obtain $|E_{\mathrm{c}}|^2 = |B|^2 |E_0|^2$.

In the first-order approximation, the scattering efficiency Q_{sca} and extinction efficiency Q_{ext} can be achieved in the quasi-static limit as follows:[35–37]

$$Q_{\mathrm{sca}} = \frac{\pi^2 (ka)^3}{4} \left| \frac{\varepsilon - \varepsilon_{\mathrm{h}} + \gamma}{\varepsilon + \varepsilon_{\mathrm{h}} + \gamma} \right|^2,$$
$$Q_{\mathrm{ext}} = \pi (ka)\, \mathrm{Im}\left[\frac{\varepsilon - \varepsilon_{\mathrm{h}} + \gamma}{\varepsilon + \varepsilon_{\mathrm{h}} + \gamma} \right]. \tag{11}$$

The absorption efficiency Q_{abs} can be defined as follows:[38]

$$Q_{\mathrm{abs}} = Q_{\mathrm{ext}} - Q_{\mathrm{sca}}. \tag{12}$$

Figure 2(a) shows the scattering efficiency *versus* incident light wavelength. We fix the radius of silk to be 60 nm based on recent experimental works[39,40] and tune the thickness of the hBN film. For a certain thickness of the hBN film t, there is always an optimal incident light wavelength to achieve the maximum value of Q_{sca}. For example, when $t = 60$ nm, $a = 60$ nm, the incident light wavelength to obtain the maximum value of Q_{sca} is approximately 7.2 μm. As the thickness of the hBN film increases, the optimal wavelength to achieve the maximum value of Q_{sca} blueshifts. The maximum value of Q_{sca} does not monotonously increase with increasing thickness of the hBN film t. It first increases as the thickness t increases and then decreases after it reaches a peak. In Fig. 2(a), we can see that the maximum value of Q_{sca} arrives at $t = 60$ nm and $a = 60$ nm when the incident wavelength $\lambda = 7.2$ μm. Therefore, in the following, we will focus on the absorption efficiency of an infrared wavelength around 7.2 μm.

Figure 2(b) shows the extinction efficiency Q_{ext} *versus* the incident light wavelength for $t = 60$ nm and $a = 60$ nm. There is an optimal incident light wavelength to obtain the maximum value of Q_{ext}. We can obtain the absorption efficiency Q_{abs} for the hBN-coated silk composite after obtaining the extinction efficiency and scattering efficiency. Figure 2(c) shows the absorption efficiency *versus* incident light wavelength with fixed $t = 60$ nm and $a = 60$ nm. The absorption efficiency Q_{abs} almost follows the same trend as Q_{ext}, as the absolute value of Q_{sca} is much smaller than that of Q_{ext}. Therefore, the peak positions of Q_{abs} and Q_{ext} are approximately $\lambda = 7.2$ μm, and the maximum value of Q_{abs} is up to 0.43 for $t = 60$ nm and $a = 60$ nm.

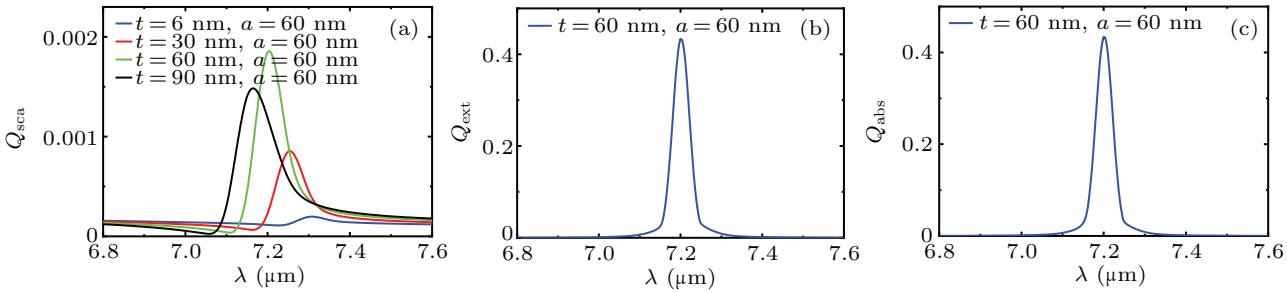


Fig. 2. (a) The scattering efficiency Q_{sca} *versus* incident light wavelength for various thicknesses of hBn film t with a fixed diameter of silk ($a = 60$ nm). (b) Extinction efficiency Q_{ext} *versus* incident light wavelength for $a = 60$ nm and $t = 60$ nm. (c) The absorption efficiency Q_{abs} *versus* incident light wavelength at $a = 60$ nm and $t = 60$ nm.

An electromagnetic wave, as the main carrier of radiative heat transfer between the body and environment, can be modified by the optical properties of textiles during the control of human thermal radiation. We calculated the dependence of the absorption efficiency in the hBN-coated silk composite on various factors to understand the intrinsic physical mechanism. Figure 3 shows that there is strong resonance absorption of the silk/hBN composite in the infrared region, which is dependent on the radius of the silk fiber, the thickness of hBN film and the wavelength of the external electromagnetic waves. Such strong absorption comes from the hyperbolic phonon polaritons in the reststrahlen band of the hBN film (see Fig. 1(b)). The hyperbolic phonon polaritons possess the feature of the hyperbolic waveguide mode in the hBN film, which leads to a large value of absorption efficiency. Figure 3(a) shows the absorption efficiency Q_{abs} *versus* the incident light wavelength for various thicknesses of hBN film with a fixed radius $a = 60$ nm. The optimal wavelength to achieve the maximum value of Q_{abs} is blueshifted as the thickness of the hBN film increases. For example, for $t = 30$ nm, $[Q_{\mathrm{abs}}]_{\mathrm{max}} = 0.19$, which is 63% of that of the case at $t = 60$ nm.

Figure 3(b) shows the absorption efficiency Q_{abs} *versus* radius of silk for different thicknesses of hBN film with fixed incident light wavelength (7.2 μm and 6.2 μm). The radius of silk ranges from 5 nm to 100 nm, which can be fabricated in the experiment. The solid lines show that Q_{abs} is very sensitive to the radius of silk for a certain thickness of hBN film at the incident light wavelength $\lambda = 7.2$ μm due to the existence of the optimal radius of silk to satisfy the ideal resonant state. We also find that the optimal radius of silk is approximately equal to the fixed thickness of the hBN film. In Table 1, the optimal radius of silk to obtain the maximum value

of Q_{abs} is 32 nm, 64 nm, and 95 nm for $t = 30$ nm, 60 nm, and 90 nm, respectively. Furthermore, the maximum value of Q_{abs} also increases as the thickness of the hBN film increases, *i.e.*, $(Q_{abs})_{max} = 0.81$ ($t = 90$ nm) > $(Q_{abs})_{max} = 0.54$ ($t = 60$ nm) > $(Q_{abs})_{max} = 0.27$ ($t = 30$ nm). However, the dashed lines show that Q_{abs} at the incident light wavelength $\lambda = 6.2$ μm is remarkably smaller than that at $\lambda = 7.2$ μm. At this light wavelength, Q_{abs} is not sensitive to the radius of the silk due to the mismatch between the resonant modes and the incident light.

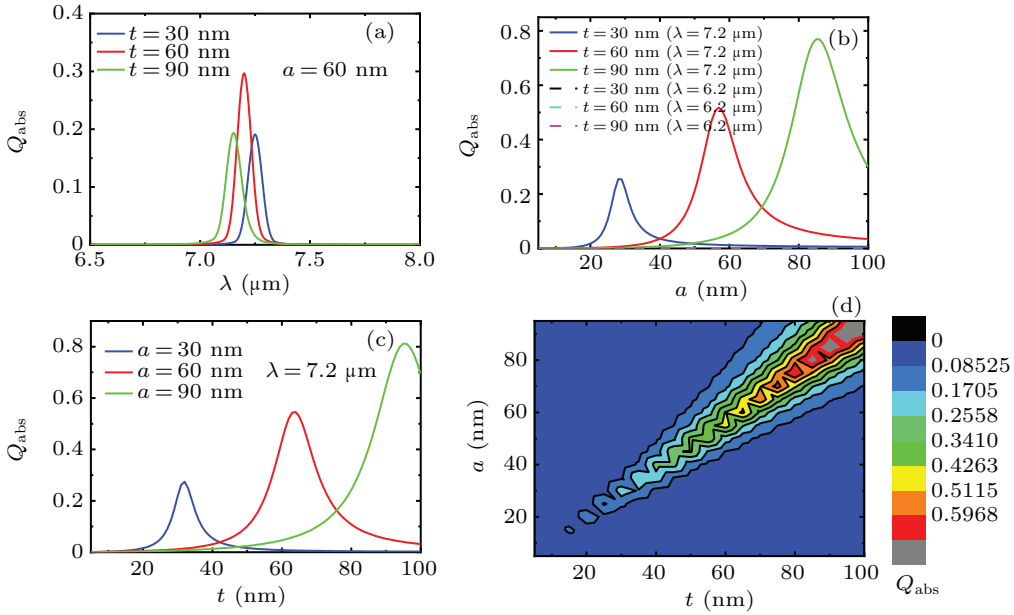


Fig. 3. (a) The absorption efficiency Q_{abs} *versus* incident light wavelength for various thicknesses of hBN film at $a = 60$ nm: $t = 30$ nm (black line); $t = 60$ nm (red line); $t = 90$ nm (green line); (b) The absorption efficiency *versus* diameter of silk a for various thicknesses of hBN film $t = 30$ nm (black line), $t = 60$ nm (red line), and $t = 90$ nm (green line) with the two wavelengths of incident light of $\lambda = 7.2$ μm (solid line) and $\lambda = 6.2$ μm (dashed line). (c) The absorption efficiency Q_{abs} *versus* thickness of hBn film t for various diameters of silk fibrils: $a = 30$ nm (black line), $a = 60$ nm (red line), and $a = 90$ nm (green line). (d) The absorption efficiency Q_{abs} *versus* the thickness of the hexagonal boron nitride film t and the radius of silk a.

Table 1. Parameters t, a_{opt}, and $(Q_{abs})_{max}$.

hBN	t (nm)	a_{opt} (nm)	$(Q_{abs})_{max}$
	30	32	0.27
	60	64	0.54
	90	95	0.81

Figure 3(c) shows the absorption efficiency *versus* the thickness of the hBN film for various radius of silk. We consider that the range of the thickness of the hBN film is 5 nm–100 nm. The absorption efficiency Q_{abs} for a certain radius of silk first increases with the thickness of the hBN film, and then decreases after it reaches a peak. The optimal thickness of the hBN film to achieve the maximum value of the absorption efficiency Q_{abs} is approximately equal to the given radius of silk, which is consistent with the results observed in Fig. 3(b). Figure 3(d) shows the absorption efficiency Q_{abs} *versus* both the thickness of the hBN film and the radius of silk to give a clear picture of the dependence of the absorption efficiency on the silk radius and the thickness of the hBN film. We can see that the maximum value of Q_{abs} increases as both the thickness of the hBN film and the silk radius increase. The maximum value of Q_{abs} can be obtained when the thickness of the hBN film is approximately equal to the silk radius, which has been observed in Figs. 3(b) and 3(c).

Before summary, we emphasize the effect of the hBN coating on the infrared absorption efficiency in silks. Figure 4 shows the absorption efficiency Q_{abs} *versus* incident light wavelength at $a = 60$ nm for both the cases with and without the hBN coating. It is obvious that the absorption efficiency Q_{abs} for the hBN-coated silk composite is much larger than that without the hBN coating in the wavelength range (6 μm$\leq \lambda \leq$ 8 μm). For instance, $Q_{abs} = 0.43$ for the case with the hBN coating is three orders larger than that without the hBN coating ($Q_{abs} = 1.3 \times 10^{-4}$). Figure 4 also shows that the absorption efficiency Q_{abs} for pure silk is 9.8×10^{-5}–4.0×10^{-4}, which is consistent with the experimental results of Ref. [41]. The experimental data in Ref. [41] show that the absorption of pure silk is from 0–4.0×10^{-3} for the wavelength range from 16 μm–18 μm. This shows the feasibility of Mie scattering theory in the description of the absorption of pure silk and functionalized silk. Therefore, it is concluded that the absorption of the silk composite is improved with the hBN coating. The enhancement of the infrared absorption in the hBN-coated silk composite comes from electromagnetic resonance coupling between the hBN coating and neighboring silk. The electromagnetic resonance can shift the high absorption efficiency of the silk/hBN composite to the mid-infrared electromagnetic wave to make it more closely

matched with the thermal radiation of the human body. A similar phenomenon is also shown in Refs. [25,42], and we have demonstrated that infrared radiation can be modulated by silk fibers coated with a thin sheet of graphene.[25] Our previous results show that this modulation arises from the electromagnetic coupling between graphene coated on neighboring silk. In addition, Zhang *et al*., have reported that infrared radiation can be tuned by a unique artificial fiber, which is also based on electromagnetic coupling between carbon nanotubes and neighboring fibers.[42]

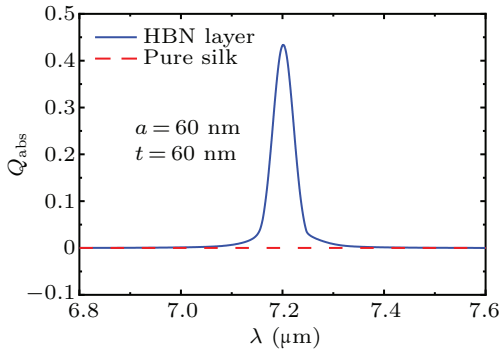


Fig. 4. The absorption efficiency Q_{abs} *versus* incident light wavelength for $a = 60$ nm and $t = 60$ nm for silk fibrils with (black line) and without hBn film coating (red line).

In summary, we studied infrared radiation in an hBN-coated silk composite. Our results show that the enhanced infrared absorption efficiency in the composite depends strongly on the hBN coating on the silk. The observed dependence on the hBN coating arises from the electromagnetic resonance coupling between the hBN coating and neighboring silk. Furthermore, by tuning the thickness of the coated hBN film and radius of silk, we could control the absorption efficiency through the composites since there is an optimal condition to satisfy the ideal resonant state. We can obtain an absorption efficiency of approximately 0.43 when the thickness of the coated hBN is approximately 60 nm. Our results provide a new way to explore an effective way to enhance the abilities of personal regulation of advanced textiles based on infrared absorption. In future work, we can make use of the out-plane phonon vibrations to improve the enhancement in the long wavelength region, and several strategies have been provided in the following section. We will provide several other ways to increase the infrared absorption efficiency as follows: (i) enhancing in-plane anisotropy, such as grating or doping. We only use an isotropic coated hBn thin film for convenience in our numerical calculation. However, as we know, the in-plane anisotropy can provide a highly confined in-plane hyperbolic phonon polariton, which can be tuned by the structural parameters and enhance the infrared absorption efficiency in a specific direction. Such an anisotropic coating has more functions and aptitudes, for example, dual-mode textiles. (ii) Cooperating with other polaritons. For example, we can coat hBn and graphene together regardless of the difficulty of preparation. In that case, the phonon polariton in hBn can interact with the plasmon polariton in graphene and form hybridized phonon-plasmon polariton modes over a wide frequency region, which can further improve the infrared absorption efficiency.

References

[1] Dolez P and Vermeersch O 2018 *Introduction to advanced characterization and testing of textiles, in: Advanced Charaterization and Testing of Textiles* (Elsevier)
[2] Zhao D, Lu X, Fan T, Wu Y S, Lou L, Wang Q, Fan J and Yang R 2018 *Appl. Energy* **218** 282
[3] Peng L, Su B, Yu A and Jiang X 2019 *Cellulose* **26** 1
[4] Hu R, Liu Y D,Shin S M, Huang S Y, Ren X C, Shu W C, Cheng J J, Tao G M, Xu W L, Chen R K and Luo X B 2020 *Adv. Energy Mater.* **10** 1903921
[5] Pakdel E, Naebe M, Sun L and Wang X 2019 *ACS Appl. Mater. Interfaces* **11** 13039
[6] Sabir T 2018 *Fibers used for high-performance apparel. in: High-Performance Apparel* (Elsevier)
[7] Wang L 2016 *Performance Testing of Textiles: Methods, Technology and Applications* (Woodhead Publishing)
[8] Hsu P C, Liu X, Liu C, Xie X, Lee H R, Welch A J, Zhao T and Cui Y 2014 *Nano Lett.* **15** 365
[9] Hazarika A, Deka B K, Kim D, Jeong H E, Park Y B and Park H W 2018 *Nano Lett.* **18** 6731
[10] Luo H, Li Q, Du K, Xu Z, Zhu H, Liu D, Cai L, Ghosh P and Qiu M 2019 *Nano. Energy* **65** 103998
[11] Zhu Y N , Luo H, Yang C Y, Qin B, Ghosh P, Kaur S, Shen W D, Qiu M, Belov P and Li Q 2022 *Light: Science & Applications* **11** 122
[12] Luo H, Zhu Y N, Xu Z Q, Hong Y, Ghosh P, Kaur S, Wu M B, Yang C Y, Qiu M and Li Q 2021 *Nano Lett.* **21** 3879
[13] Weng Q, Wang X, Bando Y and Golberg D 2016 *Chem. Soc. Rev.* **45** 3989
[14] Santin M, Motta A, Freddi G and Gannas M 1999 *J. Biomed. Mater. Res.* **46** 382
[15] Jiang X F, Weng Q, Wang X B, Li X, Zhang J, Golberg D and Bando Y 2015 *J. Mater. Sci. Technol.* **31** 589
[16] Weng Q, Wang X, Wang X, Bando Y and Golberg D 2016 *Chem. Soc. Rev.* **45** 3989
[17] Chen J, Huang X, Zhu Y and Jiang P 2017 *Adv. Funct. Mater.* **27** 1604754
[18] Gao T T, Yang Z, Chen C J, Li Y J, Fu K, Dai J Q, Hitz E M, Xie H, Liu B Y, Song J W, Yang B and Hu L B 2017 *ACS Nano* **11** 11513
[19] Min B M, Lee G, Kim S H, Nam Y S, Lee T S and Park W H 2004 *Biomaterials* **25** 1289
[20] Li H Q, Yu J S, Huang W, Shi W and Huang J 2014 *Chin. Phys. B* **23** 038505
[21] Zhang R, Yu J S, Huang J, Chen G L, Liu X, Chen W, Wang X Q and Li C R 2018 *Chin. Phys. B* **27** 055207
[22] Jing R, Wang Y, Yao Y, Wang Y, Fei X, Qi P, Lin S H, Kaplan D L, Buehler M J and Ling S J 2019 *Chem. Rev.* **119** 12279
[23] Kun L, Li P and Fan Y B 2019 *J. Mater. Chem. B* **7** 6890
[24] Zhou X H, Li D C, Wan S J, Cheng Q F and Ji B H 2019 *Acta Mech.* **230** 1413
[25] Shi L H, Huang Y, Gao L and Cheng Y 2021 *J. Elec. Mater.* **50** 592
[26] Ashal S, Sangappal Y and Sanjeev G 2016 *J. Opt.* **45** 66
[27] Zhang Z M 2020 *Nano/Microscale heat transfer*, 2nd, edn. (Springer)
[28] Zhao B, Guizal B, Zhang Z M, Fan S H and Antezza M 2017 *Phys. Rev. B* **95** 245437
[29] Zhao B and Zhang Z M 2017 *J. Heat Transfer* **139** 022701
[30] Kumar A, Low T, Fung K H, Avouris P and Fang N X 2015 *Nano Lett.* **15** 3172
[31] Alfaro-Mozaz F J, Rodrigo S G, Alonso-Gonzalez P, Velez S, Dolado I, Casanova F, Hueso L E, Martin-Moreno L, Hillenbrand R and Nikitin A Y 2019 *Nat. Commun.* **10** 42
[32] Sihvola A, Tzarouchis D C, Oijala P Y, Wallen H and Kong B B 2018 *Phys. Rev. B* **98** 235417

[33] Christensen T, Jauho A P, Wubs M and Mortensen N A 2015 *Phys. Rev. B* **91** 125414

[34] Tzarouchis D and Sihvola A 2018 *Appl. Sci.* **8** 184

[35] Li R J, Lin X, Lin S S, Liu X and Chen H S 2015 *Opt. Lett.* **40** 1651

[36] Bohren C F and Huffman D R 1983 *Absorption and Scattering of Light by Small Particles* (Wiley)

[37] Zhang K and Gao L 2017 *Opt. Express* **25** 13747

[38] Huang Y, Xiao J J and Gao L 2015 *Opt. Express* **23** 8818

[39] Zhang H R, Zhao J T, Xing T L, Lu S Z and Chen G Q 2019 *Polymers* **11** 1774

[40] Wang Q, Lin S J, Yao Q Z, Li Q Y, Hu D B, Dai Q, Weitz D A, Kaplan D L, Buehler M J and Zhang Y Y 2020 *ACS Materials Lett.* **2** 153

[41] Balcytis A, Ryu M, Wang X W, Novelli F, Seniutinas G, Du S, Wang X G, Li J L, Davis J, Appadoo D, Morikawa J and Juodkazis S 2017 *Materials* **10** 356

[42] Zhang X A, Yu S J, Xu B B, Li M, Peng Z W, Wang Y X, Deng S L, Wu X J, Wu Z P, Ouyang M and Wang Y H 2019 *Science* **363** 619